High-Temperature Corrosion Behavior of Alloy 600 and 622 Weld Claddings and Coextruded Coatings

Thermogravimetric and solid-state corrosion testing techniques were used to evaluate the corrosion behavior of nickel-based alloys

BY J. N. DUPONT, A. W. STOCKDALE, A. CAIZZA, AND A. ESPOSITO

ABSTRACT

Weld claddings are often used for corrosion protection for waterwalls in coal-fired power plants. Although these coatings provide good resistance to general corrosion, recent industry experience has shown they are susceptible to premature failure due to corrosion-fatigue cracking. The failure has been attributed, in part, to microsegregation and dilution of the weld cladding that compromise the corrosion resistance. Coextruded coatings may provide improved resistance to this type of failure due to elimination of microsegregation and dilution. In this work, the high-temperature gaseous and solid-state corrosion behavior of Alloys 600 and 622 weld claddings, and coextruded coatings were evaluated using thermogravimetric and solid-state corrosion testing techniques. The results demonstrate that Alloy 622 exhibits better corrosion resistance than Alloy 600 under the simulated combustion gases of interest, and coextruded coatings provide corrosion resistance that is significantly better than the weld claddings. The improved corrosion resistance of Alloy 622 is attributed to the higher Cr and Mo concentrations, while the better corrosion resistance of the coextruded coatings is attributed to elimination of dilution and microsegregation. Additional benefits of the coextruded coatings in terms of service performance are also likely, and include better control over coating thickness and surface finish and reduced residual stresses.

Introduction

Many coal-fired power plant operators have moved toward a staged combustion process in order to reduce boiler emissions as required by recently implemented environmental regulations. By delaying the mixing of fuel and oxygen, and thereby creating a reducing environment in the boiler, the amount of nitrous oxides (NO_x) that are released as a byproduct of coal combustion is reduced (Refs. 1, 2). The use of this staged combustion process has been found by many power plant operators to be the most cost- and time-effective method for decreasing NO_x emissions.

Prior to implementation of staged combustion, most boiler atmospheres were oxidizing, allowing for formation of protective metal oxides on waterwall tubes made out of carbon or low-alloy steels (Refs. 1, 3). Under those conditions, failure of waterwalls due to accelerated corrosion was generally not a major problem. Staged combustion boilers, on the other hand, create a reducing atmosphere in the boiler due to the lack of oxygen. Sulfur compounds from the coal are transformed into highly corrosive H_2S gas (Ref. 4). Subsequent reaction with the steel waterwall tubes leads to the formation of metal sulfides or mixed sulfides and oxides on the tube surfaces. Additionally, corrosive deposits may form on the waterwall tubes due to the accumulation of solid particles in the combustion environment, such as ash and unburnt coal. As a result of these changes, the low-alloy steel tubes are often susceptible to accelerated corrosion and unsatisfactory service lifetimes (Refs. 1, 4).

KEYWORDS

Corrosion
Weld Overlay Coating
Coextruded Coating
Ni-Based Alloys
Dilution
Microsegregation

J. N. DUPONT and A. W. STOCKDALE (aws3@lehigh.edu) *are with the Department of Materials Science and Engineering, Lehigh University, Bethlehem, Pa. A. CAIZZA and A. ESPOSITO are with Plymouth Engineered Shapes, Hopkinsville, Ky.*

The current industry solution to accelerated waterwall corrosion is to deposit a weld cladding of a more corrosion-resistant alloy on the tube. Commercially available nickel-based alloys have been used for weld claddings (Refs. 5–7). These alloys generally provide good resistance to general corrosion for this application. However, weld claddings have recently been shown to be susceptible to corrosion-fatigue cracking in many boiler environments (Ref. 6). The primary features associated with corrosion-fatigue cracking are summarized in Fig. 1 (Ref. 6). Figure 1A is a photograph of a weld cladding with extensive corrosion-fatigue cracks that were observed after approximately 18 months of service (Ref. 6). Figure 1B shows a scanning electron photomicrograph of several small cracks that were examined early in the cracking stage, and Fig. 1C shows the distribution of alloying elements across the dendritic substructure of the overlay. Figure 1D provides a lower-magnification view that demonstrates the cracks initiate at the valley of the weld ripple. The dendrite cores in the cladding exhibit a minimum in alloy concentration due to the relatively rapid solidification conditions associated with welding (Ref. 7). As a result, the corrosion rate is accelerated in these regions and localized attack occurs at the dendrite cores. These localized penetrations form stress concentrations that eventually grow into full-size corrosion-fatigue cracks under the influence of service-applied stresses. As shown in Fig. 1D, most cracks initiate in the valley of surface weld ripples where an additional stress concentration exists. The high residual stress that results from welding also probably contributes to the cracking problem. In addition, dilution from the underlying tube substrate, which results in reduced alloy content of the cladding, compromises the corrosion resistance of the cladding.

It is important to note that the primary factors that contribute to corrosion-fatigue cracking (weld ripple, microsegregation, high residual stresses, and dilution) are all associated with the localized

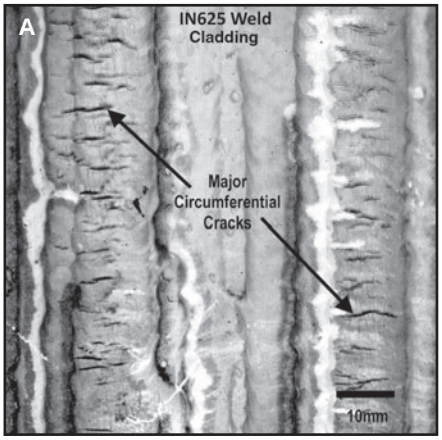

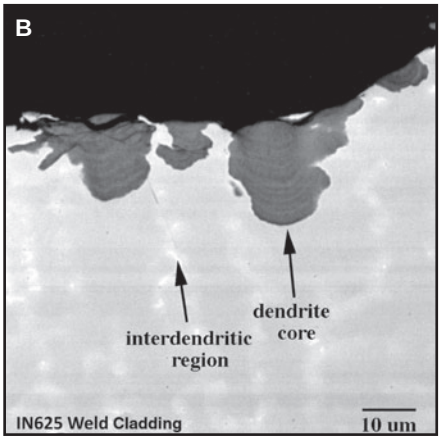

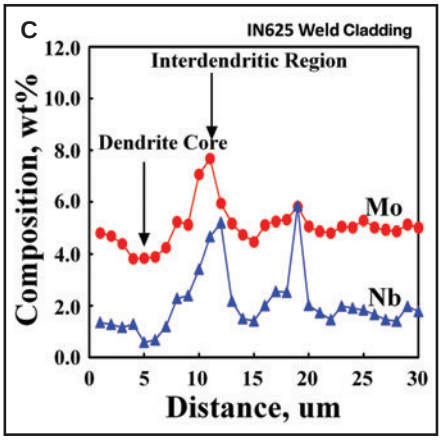

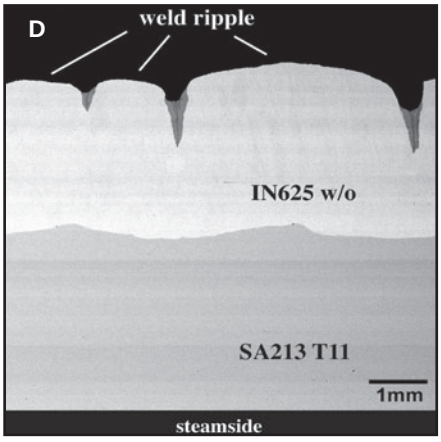

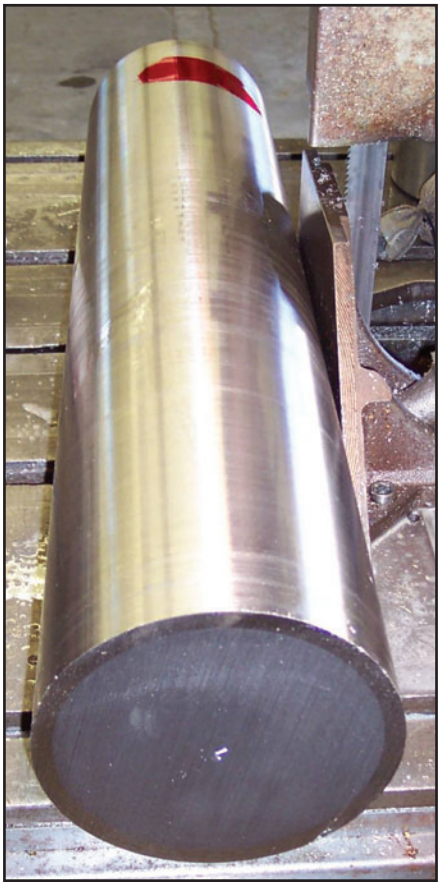

Fig. 1 — A — Photograph of an IN625 weld cladding with extensive circumferential cracks; B — cross-sectional scanning electron photomicrograph of several small cracks early in the cracking stage; C — distribution of alloying elements across the dendritic substructure of the IN625 weld cladding; D — photograph showing crack initiation at the valley of the weld ripple.

Fig. 2 — Photograph of starting bimetallic billet showing the inner steel substrate and outer nickel alloy layer prior to coextrusion. The starting billet had a diameter of approximately 6 in. and a length of about 2 ft.

heating, melting, and solidification of the welding process. As such, use of a coating that can be applied uniformly on the substrate surface in the solid state (i.e., without the need for localized heating) should help mitigate these problems and improve the cracking resistance of the coating. Thus, there is a need to develop alternative coating technologies that avoid these drawbacks. Coextruded coatings provide a potential alternative because they are produced completely in the solid state and therefore require no melting and resolidification. In this work, the high-temperature corrosion resistance of two nickel-based alloys (600 and 622) were investigated in the form of both coextruded coatings and weld claddings. The counterpart wrought product form was also tested for Alloy 600 for comparison.

Experimental Procedure

Three types of samples were corrosion tested: coextruded coating, wrought alloy (for Alloy 600 only), and weld cladding. Coextruded tubes were manufactured at Plymouth Engineered Shapes using an outer layer of either Alloy 600 or 622 and a 1.25Cr-0.5Mo (SA213-T11) steel substrate. The composition of the Ni-based alloys and the steel are provided in Table 1. The steel substrate and nickel alloy outer layer were joined by an explosion welding process prior to coextrusion. As shown in Fig. 2, the substrate and outer layer had a starting diameter of 6 in. and length of about 2 ft. The bimetallic billet was heated to 1040°C prior to coextrusion, and the coextrusion occurred in approximately 5 s. Figure 3 shows an example of the final bimetallic tube produced after coextrusion that has an outside diameter of 2.5 in. with a 0.250-in. wall thickness and a coating thickness of 0.085 in. The final tube length was approximately 20 ft. Simulated weld claddings were fabricated by mixing (by weight) 10% of an Alloy 285 Grade C steel substrate (this alloy is similar to those typically used for waterwall tubes) with 90% of Alloy 600 or 622. The 10% steel was added to simulate a typical dilution level of a commercial weld cladding. (It is recognized that Alloy 600 is not available in wire form for use as a weld cladding. However, the weld cladding samples were prepared and tested here to provide a direct comparison to the coextruded coating of the same composition.) The mixture was then melted and resolidified in an arc button melter, which essentially duplicates the chemical composition and thermal conditions used to make weld claddings. This process has been used extensively for preparing and corrosion testing weld cladding samples (Ref. 8). Gaseous corrosion testing was carried out at 600°C for 100 h in a Netzsch thermogravimetric balance. The gas used for the corrosion tests was modeled after a typical low-NO_x environment and consisted of the following mixture (Ref. 8): 10%CO-5%CO_2-2%H_2O-0.12%H_2S-N_2 (vol-%). Corrosion samples were acquired from the coating of the bimetallic tube by completely machining away the underlying steel substrate.

The Alloy 622 weld cladding and coextruded samples were also tested under solid-state corrosion conditions. (Alloy 600 was not evaluated under solid-state conditions, since the gaseous corrosion results demonstrated that Alloy 622 had superior corrosion resistance.) Samples that were ¾ × ¾ × 5/16 in. were machined from the coextruded tube and the weld cladding. A quartz ring was placed on top

Fig. 3 — A section of the final bimetallic tube produced after coextrusion. The tube has an outside diameter of 2.5 in. with a 0.250-in. wall thickness and a coating thickness of 0.085 in. The final tube length was approximately 20 ft.

of the samples, and 1680 mg of FeS_2 powder was poured into the quartz ring. The FeS_2 powder simulates the iron sulfide that is often deposited on waterwall surfaces in the form of coal particles that are not completely combusted. The iron sulfide will oxidize at high temperature and subsequently release sulfur gas that corrodes the underlying coating (Refs. 9, 10). The samples were placed in a furnace and heated to 600°C for 50, 150, and 300 h (separate samples were used for each exposure time). The samples were then examined in cross section to reveal the depth of attack and corrosion morphology after each exposure time. This test has been shown (Ref. 8) to simulate the solid-state corrosion that occurs when deposits form on the waterwall tubes in service. Corrosion test coupons from the gaseous and solid-state tests were mounted under vacuum in cold setting epoxy and ground through 600 grit with a SiC abrasive. The samples were then polished to a 0.05–μm surface finish. Post-test imaging of corrosion scales was conducted via light optical microscopy and scanning electron microscopy on a Hitachi 4300 scanning electron microscope (SEM) equipped with an energy-dispersive spectrometer.

Results

Figure 4 shows photographs that compare the coating surface finish and thickness uniformity of the coextruded coating (Fig. 4A, B) and a weld cladding typically used for this application (Fig. 4C, D). The weld cladding exhibits the typical surface ripples associated with solidification and a relatively uneven coating thickness. The coextrusion process provides a relatively smooth surface finish and more uniform coating thickness. Elimination of the weld ripple is significant, since the valleys of the weld ripple present stress concentrations that exacerbate corrosion-fatigue crack initiation (Ref. 6). The more uniform coating thickness and improved surface finish associated with the coextruded coating eliminates this form of stress concentration and should therefore be more resistant to initiation of corrosion-fatigue cracks.

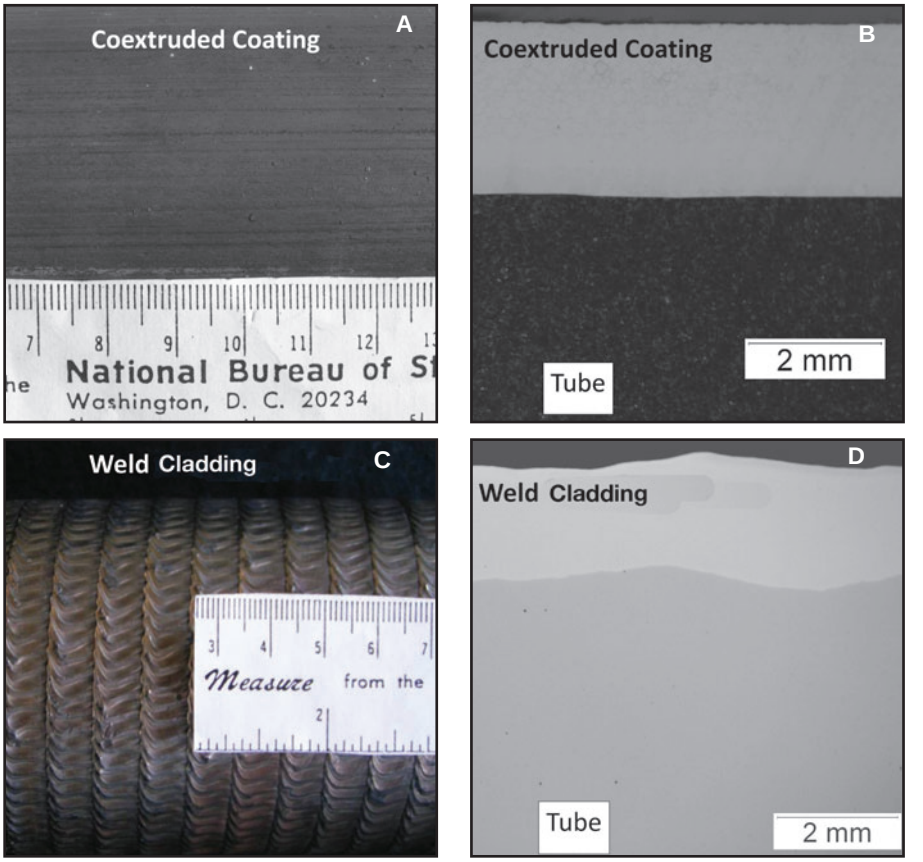

Fig. 4 — Comparison of coating surface finish and thickness uniformity of the following: A, B — Coextruded coating; C, D — a weld cladding typically used for this application.

Figure 5 shows the thermogravimetric analysis results from the gaseous corrosion testing. These results compare the normalized weight gain of the weld cladding and coextruded coating. Corrosion results from the alloy in the wrought condition are also shown for Alloy 600 for comparison. Good corrosion results are indicated by relatively low weight gains, and the slopes of the lines are an indication of the corrosion rates. The coextruded coating clearly shows improved corrosion resistance over the weld cladding, and the corrosion resistance of the wrought alloy and coextruded coating for Alloy 600 is comparable. Also note that Alloy 622 demonstrates better corrosion resistance (i.e., lower weight gains) than Alloy 600.

Figure 6 shows SEM cross-sectional photomicrographs of the corrosion coupons from the gaseous corrosion tests. These samples reveal an outer scale in addition to an inner corrosion scale that formed adjacent to the coating surface during corrosion testing. It is important to note that, due to the large differences in corrosion scale thickness, the photomicrographs acquired from the coextruded coating (Fig. 6A, B) are generally taken at a higher magnification than those of the weld cladding (Fig. 6C, D). The inner corrosion scale that formed on the coextruded sample is signifi-

Table 1 — Composition of the Ni-Based Alloys and Steel Used to Make the Coextruded Tubes (all values are given in wt-%)

	622	600	T11
C	0.002	0.06	0.12
Co	0.81	0.06	—
Cr	21.3	16	1.22
Fe	3.7	7.47	—
Mn	0.25	0.36	0.52
Mo	13.1	—	0.52
Ni	Bal	Bal	0.02
P	0.012	—	0.009
S	0.002	0	0.026
Si	0.03	0.34	0.62
V	0.02	0.04	0.006
W	2.8	—	—
Nb	—	0.01	—
Ta	—	0.01	—
Ti	—	0.22	—
Al	—	0.2	0.029
Cu	—	0.03	0.02
Cs			0.002
N			0.005
Sn			0.002

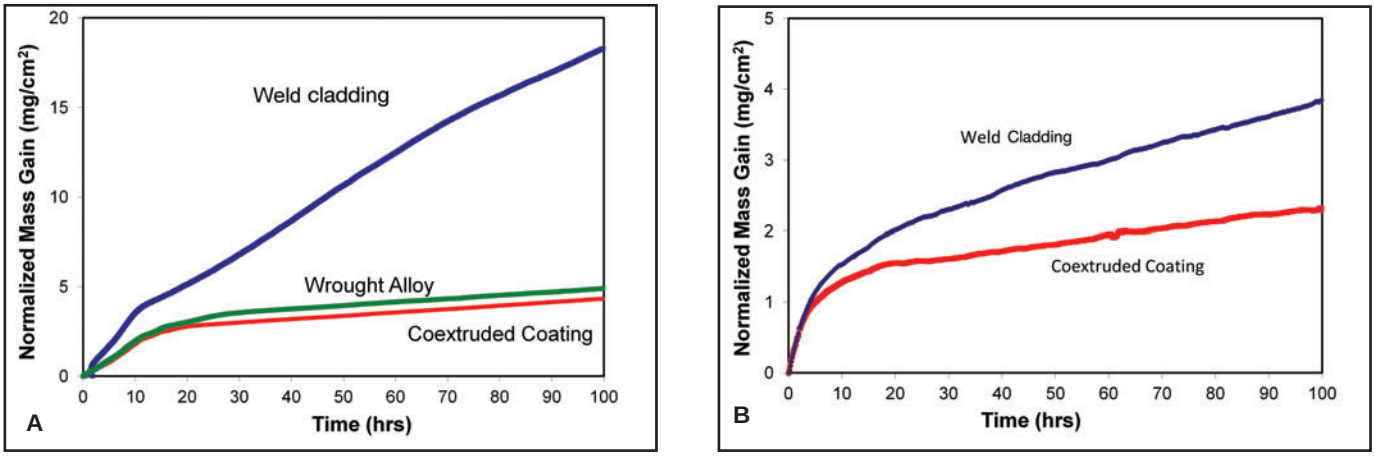

Fig. 5 — Thermogravimetric results from the gaseous corrosion testing. A — Alloy 600; B — Alloy 622.

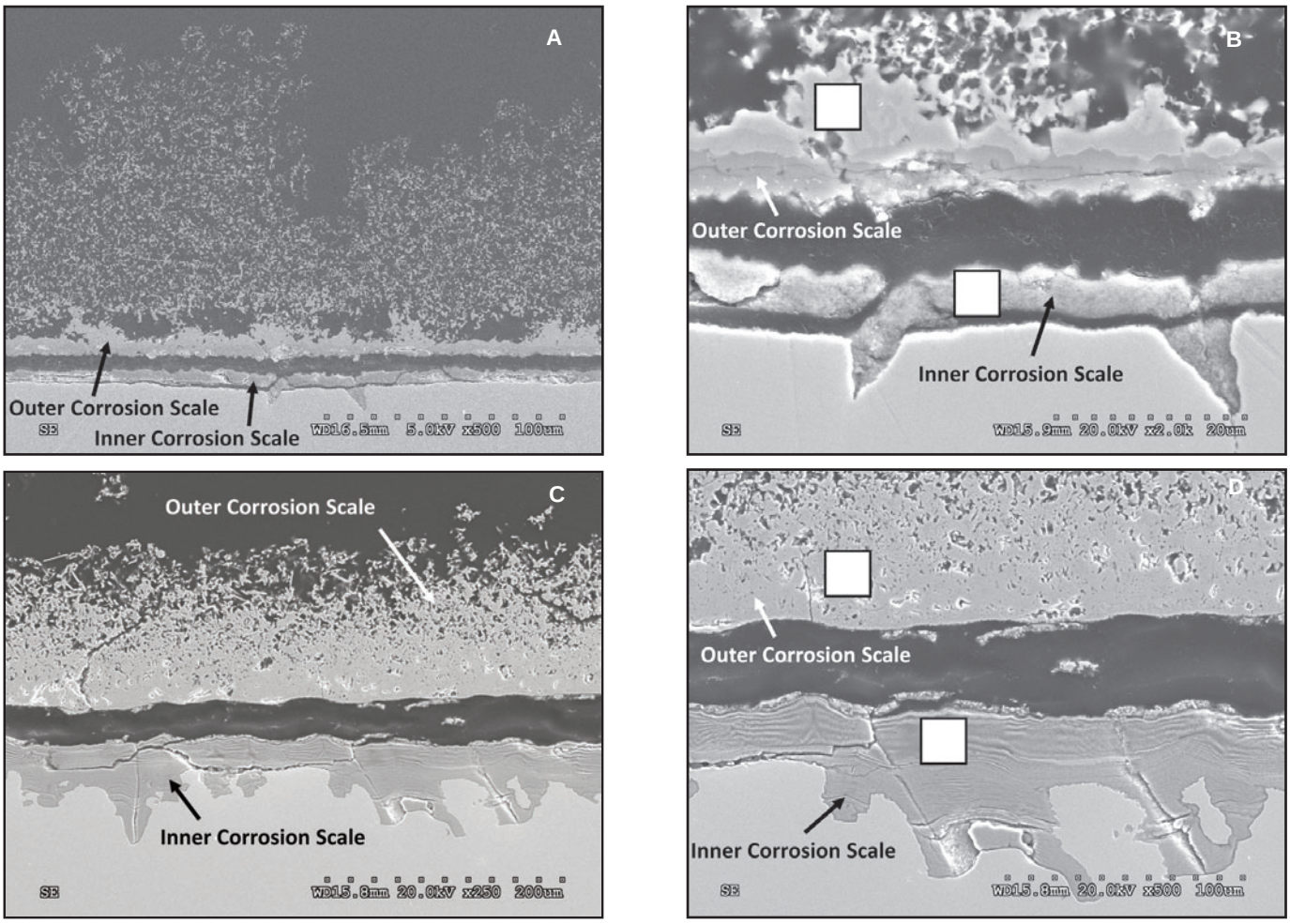

Fig. 6 — SEM cross-sectional photomicrographs of the corrosion coupons from the gaseous corrosion tests of Alloy 600 for the coextruded coating (Fig. 6A, B) and weld cladding (Fig. 6C, D).

cantly thinner than the inner scale that formed on the weld cladding. Figure 6A, which was acquired from the coextruded sample, was taken at the same magnification as Fig. 6D acquired from the weld cladding, and the differences in scale thickness are readily apparent when these two images are compared. Also note that corrosion has occurred more uniformly on the coextruded coating compared to the weld cladding. The differences in scale thickness are consistent with the differences in the weight gain results shown in Fig. 5, where the weld cladding exhibited a higher weight gain (due to the higher corrosion rate and concomitantly larger scale thickness). A thinner inner corrosion scale is preferred, as this indicates that the scale provides better protection between the corrosion environment and underlying coating surface.

Figure 7 shows EDS spectra collected from the corrosion scales that formed on the gaseous corrosion samples. The locations that the EDS scans were acquired from are shown as white boxes in Fig. 6B, D. (In each case, EDS spectra acquired from the area between the inner and outer

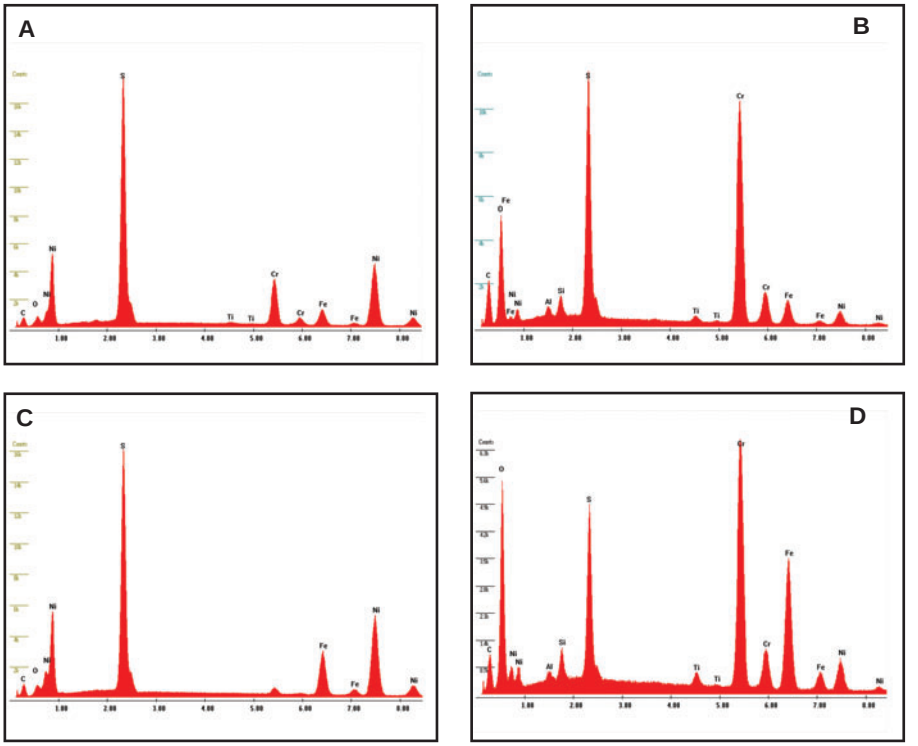

Fig. 7 — EDS spectra acquired from gaseous corrosion samples of Alloy 600. A — Top surface scale of the coextruded coating; B — inner surface scale of coextruded coating; C — top surface scale of the weld cladding; D — inner surface scale of weld cladding.

scales were observed to reveal the presence of carbon and oxygen, indicating that it is merely the mounting material used to prepare the samples. This occurs when the inner and outer scales separate during preparation.) For each coating type, the outer scales are rich in nickel and sulfur. The inner scales of each sample are also similar and reveal the presence of a chromium-rich mixed oxygen-sulfur scale.

Figure 8 shows the extent of corrosion that occurred during the solid-state corrosion testing for the Alloy 622 weld cladding and coextruded coatings. A significant amount of corrosion scale can be observed on the surface of each sample. The amount of scale on the surface is indicative of the severity of the corrosive attack. The corrosion resistance of the weld cladding and coextruded coatings are somewhat similar up to 50 h of exposure. However, at 150 and 300 h, the depth of attack is greater on the weld cladding. Also note that the weld cladding exhibits localized corrosion penetrations (arrows in Fig. 8F) while corrosion on the coextruded coating is uniform.

Figure 9 shows the 300-h corrosion sample of the weld cladding after it was etched to reveal the dendritic substructure. Note that preferential corrosion has occurred at the dendrite cores (arrows). Figure 10 provides an EDS line scan that was acquired across the dendritic substructure of the weld cladding. As expected (Refs. 6, 7), the dendrite cores are depleted in Mo, with Mo concentration levels down to ~ 11 wt-% (the nominal Mo concentration of the filler metal is ~ 13 wt-%). Note that the Ni segregates in the opposite direction compared to Mo (i.e., to the dendrite cores). The particularly high Mo level of ~ 38 wt-% (at a position of ~ 3 μm) is coincident with Ni depletion down to ~ 28 wt-% and is associated with the electron beam interacting with Mo-rich interdendritic phase.

Figure 11 shows the microstructure of the coextruded coating, and an EDS line scan acquired across several grains of the coating is shown in Fig. 12. The coextruded coating exhibits a uniform, equiaxed grain structure and a uniform distribution of alloying elements.

Discussion

The corrosion results demonstrate the effect of the coating process on the resultant corrosion resistance. For each alloy, the coextruded coatings provide significantly better corrosion resistance than the weld claddings. Since the alloy is the same in each case, the reduced corrosion resistance of the weld cladding must be attributed to differences in processing that affect the microstructure. This is confirmed by the results shown for Alloy 600 in which a wrought alloy was also tested for comparison — Fig. 5A. Note that the wrought alloy and coextruded coating exhibit essentially identical corrosion rates. This indicates the coextrusion process has no detrimental effect on the inherent corrosion resistance of the wrought alloy. This is consistent with the observed microstructure (Fig. 11) and distribution of alloying elements (Fig. 12) observed for the coextruded coating. The equiaxed grain structure and uniform distribution of alloying elements is similar to that observed for a wrought alloy, so the corrosion resistance is also expected to be similar, as observed in Fig. 5A.

The differences in corrosion resistance among the two alloys and coating types evaluated here can be understood by considering differences in their composition. It is well known that Cr and Mo additions significantly improve the sulfidation resistance of Ni-based alloys (Refs. 11, 12). For example, Chen and Douglass (Refs. 11, 13) evaluated the effect of Mo additions on the sulfidation resistance of Ni-Mo alloys at 600°C at a sulfur partial pressure of 0.01 atm P_{S2}. Five alloys were evaluated, including Ni, Ni-10wt-%Mo, Ni-20wt-%Mo, Ni-30wt-%Mo, and Ni-40wt-%Mo. The parabolic rate constant decreased by four orders of magnitude as the Mo content was increased to 40 wt-% Mo. Similar reductions in the parabolic rate constant were also observed for Ni-Cr alloys tested by Mrowec et al. (Refs. 12, 14). The sulfidation behavior of Ni with up to 82 at-% Cr was evaluated in a sulfur partial pressure of 1 atm P_{S2} at 600°C. The parabolic rate constant decreased by three orders of magnitude as the chromium content was increased up to 82 at.-% Cr. These results demonstrate that the corrosion resistance of Ni-based materials is improved by alloying additions of Cr and Mo. Thus, the improved corrosion resistance of Alloy 622 over Alloy 600 is attributed to the higher Cr and Mo concentration of Alloy 622.

The improved corrosion resistance of the coextruded coatings can be attributed to two factors. First, the weld cladding exhibits a 10% reduction in key alloying elements (e.g., Cr and Mo) due to 10% dilution with the steel substrate, and a reduction in the concentration of these elements will produce an increase in the corrosion rate. The 10% dilution value used for these tests represents a lower limit on the dilution level for commercially applied weld claddings. The dilution level in field-applied weld claddings can often be higher than this, and the corrosion resistance can be reduced even further as a result. Such dilution effects do not occur with the coextruded coating because there is no melting and mixing associated with this process. Although there is localized solid-state diffusion across the coating/substrate interface during processing, there is no bulk change in coating composition. Second, the weld cladding exhibits mi-

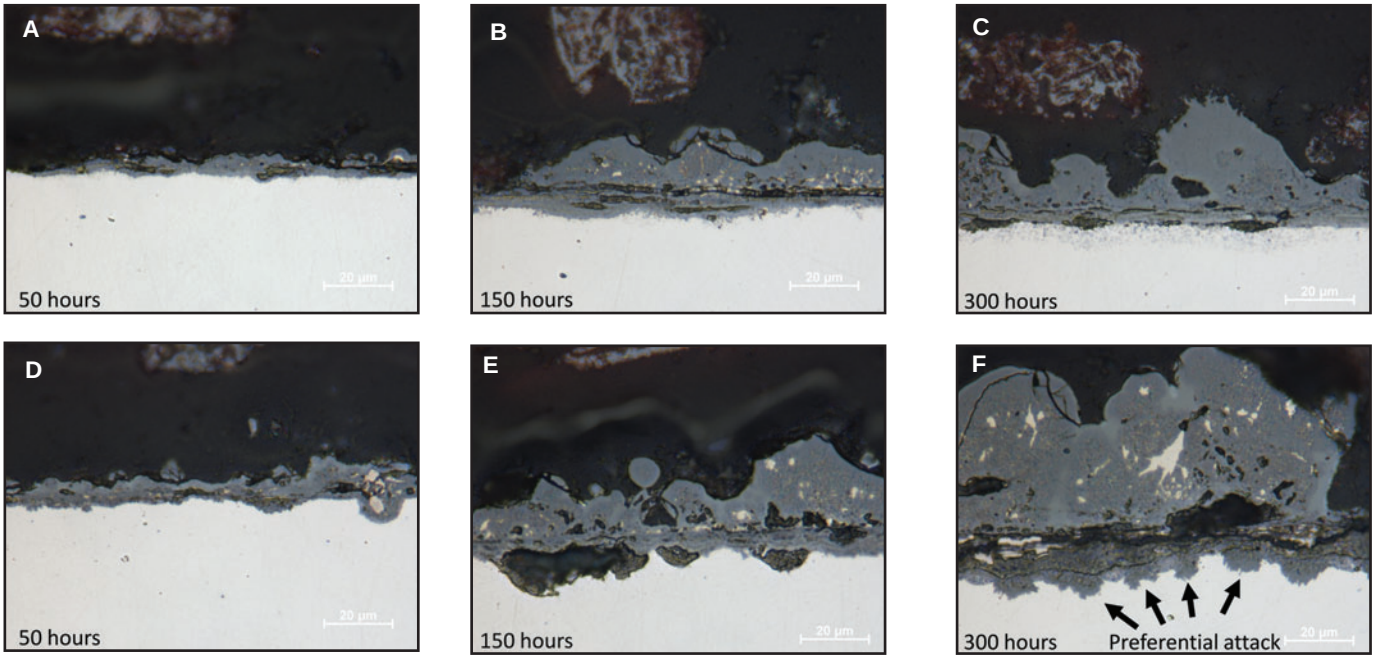

Fig. 8 — Light optical photomicrographs showing the extent of corrosion that occurred during solid-state corrosion testing for the following: A, B, C — Alloy 622 coextruded; D, E, F — weld cladding coatings.

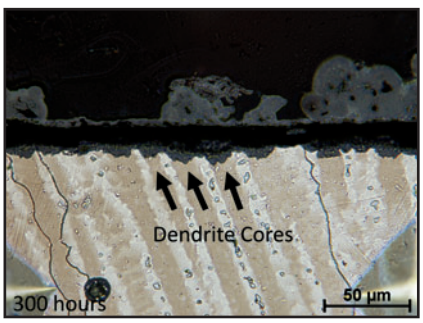

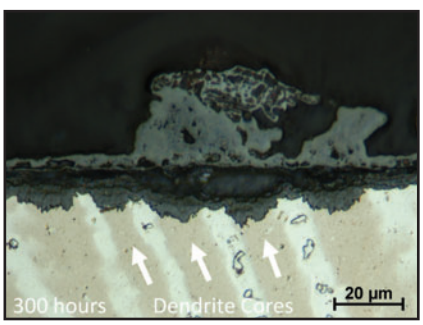

Fig. 9 — Light optical photomicrographs of the 300-h corrosion sample of the weld cladding after it was etched to reveal the dendritic substructure. Note that preferential corrosion has occurred at the dendrite cores (arrows).

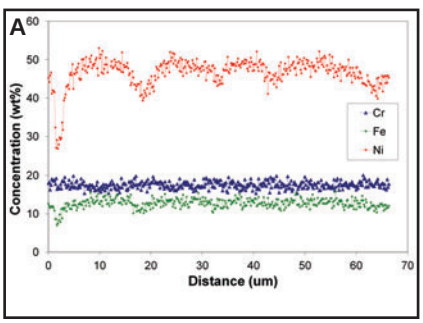

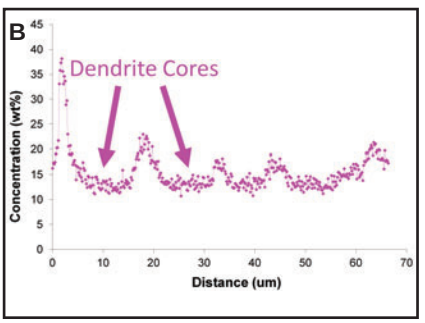

Fig. 10 — A — EDS line scan acquired across the dendritic substructure of the weld cladding showing the composition profiles for Fe, Ni, and Cr; B — EDS line scan acquired across the dendritic substructure of the weld cladding showing Mo depletion at the dendrite cores.

crosegregation in which the dendrite cores are depleted in alloying elements (particularly of Mo) that are important for corrosion protection (Ref. 15). As a result, corrosion occurs more rapidly at the alloy-depleted cores, thus leading to the preferential corrosive attack at the dendrite cores observed in Figs. 6C, 6D, and 9.

It is worth noting that the coextruded (and wrought) Alloy 600 provides corrosion resistance that is nearly comparable to the Alloy 622 weld cladding, suggesting that Alloy 600 may be useful as a coextruded coating. However, the objective here is to develop a coating/process combination that provides performance better than the current industry standard (622 weld cladding). Thus, the use of Alloy 600 as a coextruded coating does not appear warranted based on this consideration.

These results indicate that coextruded coatings should provide significant benefits over weld claddings for corrosion protection in fossil-fired boilers. (It should be recognized that weld claddings can be applied in the field or the shop, while coextruded coatings can only be applied in the shop.) Reduction or elimination of failures due to corrosion-fatigue cracking will require the development of coatings with improved resistance to both general corrosion and localized corrosion that occurs due to microsegregation. Other factors that promote corrosion-fatigue crack initiation should also be avoided, such as surface irregularities and high residual stresses. Coextruded coatings provide several advantages over the weld claddings in these regards. First, the coextruded coatings will not exhibit dilution and microsegregation that compromise corrosion resistance. The weld claddings also exhibit surface ripples associated with the solidification process, and the valleys of these ripples are sources of stress concentration that can contribute to corrosion-fatigue cracking (Ref. 6). In contrast, the coextruded coatings have a uniform coating thickness and smooth surface finish that should help eliminate localized stress concentrations that initiate corrosion-fatigue cracks. Weld claddings also develop very high levels of residual stress that are associated with localized heating and cooling. The residual stress level is generally on the order of the yield strength of the alloy (Ref. 16), and this may also be a contributing factor to the corrosion-fatigue problem. In contrast, the heating and cool-

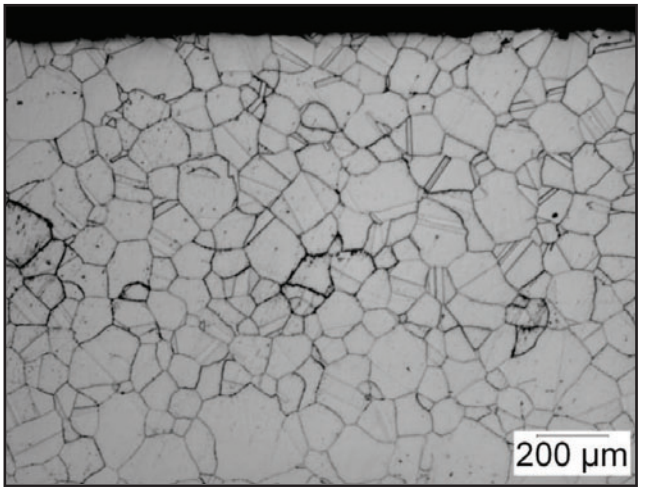

Fig. 11 — Light optical photomicrograph showing the microstructure of the coextruded coating.

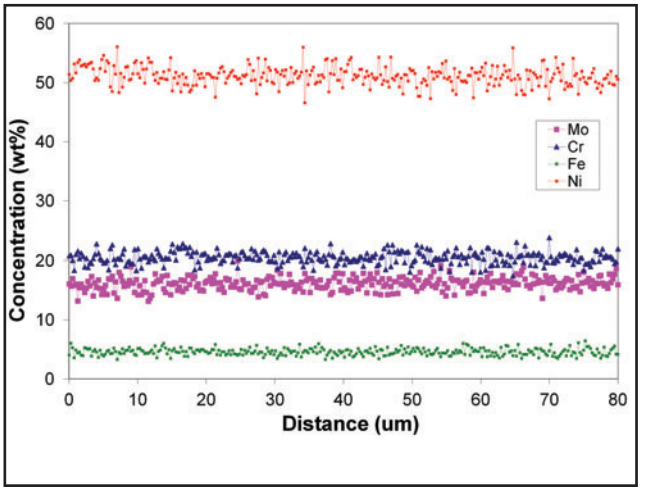

12 — EDS line scan acquired across several grains of the coating.

ing cycles experienced during coextrusion are less severe and more uniform. As a result, the residual stresses should be significantly reduced. Corrosion-fatigue testing and field tests are currently in progress to verify this expected level of improvement and will be reported in the future.

Summary

The high-temperature corrosion resistance of Alloys 600 and 622 weld claddings and coextruded coatings was evaluated in this work. A wrought sample of Alloy 600 was also corrosion tested for comparison. The results demonstrate: 1) Alloy 622 exhibits better corrosion resistance than Alloy 600; and 2) coextruded coatings provide corrosion resistance that is significantly better than the weld claddings. The improved corrosion resistance of Alloy 622 is attributed to the higher Cr and Mo concentrations. The improved corrosion resistance of the coextruded coatings relative to the weld cladding is attributed to elimination of dilution and microsegregation in the coextruded coating. Additional benefits of the coextruded coating in terms of service performance are also likely, and include better control over coating thickness/surface finish and reduced residual stresses.

Acknowledgments

The authors gratefully acknowledge financial support through the National Science Foundation Center for Integrated Materials Joining Science for Energy Applications, Grant IIP-1034703, and PPL Corp., Contract 00474836. Useful technical discussions with Ruben Choug and Robert Schneider of PPL Corp. are also gratefully appreciated.

References

1. Jones, C. 1997. *Power* January/February, pp. 54–60.
2. Whitaker, R. 1982. *EPRI Journal,* pp. 18–25.
3. Urich, J. A., and Kramer, E. 1996. FACT (American Society of Mechanical Engineers), Vol. 21, pp. 25–29.
4. Kung, S. C., and Bakker, W. T. 1997. *Mater. High Temp.* 14: 175–182.
5. Smith, G. D., and Tassen, C. S. 1989. *Mater. Perf.* 28: 41–43.
6. Luer, K., DuPont, J. N., Marder, A. R., and Skelonis, C. 2001. *Mater. High Temp.* 18: 11–19.
7. DuPont, J., Lippold, J., and Kiser, S. 2009. *Welding Metallurgy and Weldability of Nickel-base Alloys.* p. 440, Hoboken, N.J.: John Wiley & Sons.
8. Regina, J. R., DuPont, J. N., and Marder, A. R. 2004. Corrosion behavior of Fe-Al-Cr alloys in sulfur- and oxygen-rich environments in the presence of pyrite. *Corrosion*. pp. 501–509.
9. Bakker, W. 1998. *Waterwall Wastage in Low Nox Boilers: Root Cause and Remedies.* TR-111155.
10. Kung, S., and Bakker, W. 2000. Waterwall corrosion in coal-fired boilers a new culprit: FeS. *Corrosion 2000*. pp. 26–31. NACE International.
11. Chen, M. F., and Douglass, D. L. 1989. The effect of molybdenum on the high-temperature sulfidation of nickel. *Oxid. Met.* 32: 185–206.
12. Mrowec, S., Werber, T., and Zastawnik, M. 1966. The mechanism of high temperature sulfur corrosion of nickel-chromium alloys. *Corros. Sci.* 6: 47–68.
13. Gleeson, B., Douglass, D. L., and Gesmundo, F. Effect of niobium on the high-temperature sulfidation behavior of cobalt. *Oxid. Met.* 31: 209–236.
14. Czerski, L., Mrowec, S., and Werber, T. 1962. Kinetics and mechanism of nickel-sulfur reaction. *Journal of the Electrochemical Society* 109: 273–278.
15. Deacon, R. M., DuPont, J. N., and Marder, A. R. 2007. *Materials Science & Engineering A* Vol. 460–461, pp. 392–402.
16. Kou, S. 2002. *Welding Metallurgy.* p. 461, Hoboken, N.J.: John Wiley & Sons.